Hydrogen diffusion and trapping in bodies undergoing rolling contact

Nicholas Winzer[a] (corresponding author), nicholas.winzer@iwm.fraunhofer.de, Tel: +49(0)7615142256, Fax: 49(0)7615142503

Iyas Khader[a,b], iyas.khader@iwm-extern.fraunhofer.de

[a] Fraunhofer Institute for Mechanics of Materials IWM, Wöhlerstraße 11, D-79115 Freiburg, Germany

[b] Department of Industrial Engineering, German Jordanian University, P.O. Box 35247, 11180 Amman, Jordan

Abstract

Diffusion and trapping of hydrogen (H) in bodies undergoing combined rolling and sliding contact has been evaluated using finite element analysis. The elastic stress-strain conditions of the bodies were calculated in 3D for a single rotation. The stresses were then used to simulate H diffusion in a single plane close to the contact point over large numbers of cycles. The distribution of deformation-induced defects was approximated by relating an isotropic hardening model to the dislocation density. The influence of the defects on H diffusion was evaluated using the McNabb & Foster model assuming local equilibrium as per Oriani. The influence of residual stresses, such as those occurring in bearings after manufacturing, and frictional heating were also considered. The results show that slightly elevated H concentrations occur in the plastic zone conditions and that the increase in H concentration is due to trapping by deformation-induced defects. The influence of stress-assisted diffusion is small due to: (i) the short period of time a point on the contact surface spends under load relative to the period of rotation; and (ii) the spatial separation of the hydrostatic and von Mises components of the contact stresses.

Keywords: rolling contact fatigue; finite element modelling

1   Introduction

Hydrogen-assisted rolling contact fatigue (HA-RCF) is often proposed as a cause of premature degradation of rolling element bearings by "brittle flaking" or "white structure flaking". There is a consensus in the literature that hydrogen is generated by degradation of the lubricant by some tribo-chemical reaction [1,2,3,4,5,6] and absorbed by the bearing material as atomic hydrogen (H). However, there is general disagreement regarding the mechanism that promotes the H generation and ad/absorption (a prevailing proposal is that the critical process is the catalysis of the decomposition reaction by bare metal surfaces exposed by sliding contact [2]) and the influence of H on fatigue damage processes. Critical to understanding the latter is developing an understanding of the diffusion and trapping of H inside the bearing material. Due to the complicated natures of the contact stresses and the distribution of deformation-induced defects that may act as H traps, this is less intuitive than other problems involving stress-assisted H diffusion. For example, continuum models have shown that H accumulates at regions of elevated tensile stresses such as those occurring around crack tips [7,8,9,10,11]. In contrast, contact stresses are mostly compressive in nature and thus tend to repel H. This is further complicated by the existence of residual stresses resulting from machining and hardening processes, which may be compressive or tensile. Disregarding the influence of H traps, it is not immediately clear why H should remain, let alone accumulate, in the region where fatigue damage processes are occurring. Thus, it was anticipated that deformation-induced defects acting as H traps would have a considerable influence on the H-distribution in bodies undergoing rolling contact.

The aim of the described work was to provide a preliminary analysis of stress-assisted H diffusion and trapping under conditions typical of those occurring in bodies undergoing rolling contact. We chose to simulate experiments currently being carried out at IWM using double-roller type specimens, in which premature rolling contact fatigue failure has been shown to occur for H-charged samples and for which test parameters were available. One of the challenges associated with simulation of such systems is the competing demands of modelling of the stress-strain condition and of H diffusion and trapping. Although analytical solutions for the elastic stress condition of the material exist [12,13,14,15,16], these are complex and do not consider the combined influences of rolling and sliding contact. A more accurate depiction of the stress-strain state requires a detailed 3-

dimensional discretisation of the specimen geometry, the solutions to which are computationally intensive. In contrast, modelling of H diffusion and trapping over large numbers of cycles requires very high computational expediency. In the present work, this conflict was resolved through the implementation of a multiscale framework, in which the elastic stresses were calculated in 3D using ABAQUS for a single rotation and exported along with the nodal data into a bespoke FE code programmed in Python for determining the distribution of H in a single radial plane under isothermal conditions over large numbers of cycles. This spatial separation of the stress and H diffusion problems necessitated the assumption that the hardening behaviour of the material follows an isotropic hardening power-law. A consequence of this assumption is that a steady-state distribution of defects is attained after the first few rotations (the "shakedown" period), and remains constant throughout the period of H diffusion. The results, though not constituting a thorough treatment of plasticity effects, show that the H distribution in the near-contact region is relatively constant, with slight increases in H concentration due to H trapping at deformation-induced defects.

2   Details of model

2.1   *Evaluation of the stress-strain condition*

Rolling contact stresses were calculated for a twin-disc test configuration using a coupled thermal-mechanical three-dimensional finite element simulation in ABAQUS. Due to the symmetry of the system, only one half of the geometry was modelled. The model was comprised of a crowned disc with a circular profile rolling on the surface of a flat roller with a predefined normal force and slip rate under continuous oil lubrication. The dimensions of the rollers are shown in Figure 1. The disc and roller were rotated at 300 and 270 rpm respectively, i.e. with a slip ratio of approximately s = 0.105, under a constant normal load of 1kN.
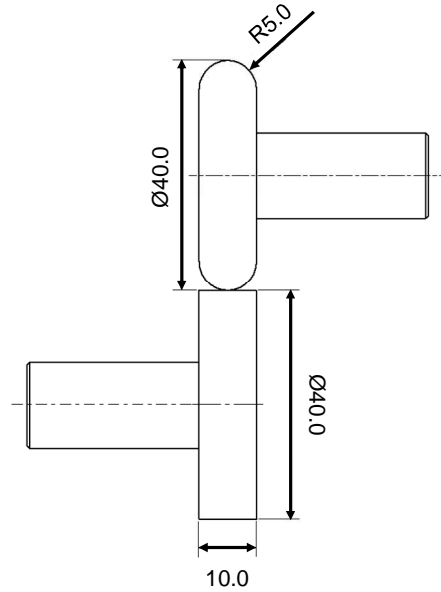
Figure 1 – Dimensions of the crowned and flat roller (mm)

Coulomb friction with a constant frictional coefficient of $\mu = 0.08$ was assumed based on the average frictional coefficient determined through a series of measurements carried out using a twin-disc tribometer. Isotropic linear elastic material behaviour for 100Cr6 (SAE52100) steel was assumed for both bodies. This ensured an adequate approximation of a quasi-Hertzian contact condition.

In order to resolve contact stresses with an acceptable accuracy while maintaining a reasonable size, a dense mesh was created in the vicinity of the contact surfaces only. The average element size adjacent to the plane of symmetry was $60\times60\times20$ µm. Eight-node first-order hexahedral elements with displacement and temperature degrees of freedom (C3D8T) were used to discretise the geometry.

The frictional energy dissipation was calculated from the frictional stress and slip rate. The distribution of the heat between the interacting surfaces was assumed to be identical, whereas the fraction of dissipated energy converted into heat (mechanical to thermal) was assumed to be 90% of the overall frictional energy, in order to account for heat transfer losses by natural convection and lubrication. Thermo-mechanical properties were linearly interpreted from those listed in Table 1.

The nodal data (coordinates and stresses) were extracted from a plane parallel to a cutting surface along the cross section of the contact ellipse (X-Y plane in Figure 2) and exported into the H diffusion model.

Table 1 – Thermo-mechanical parameters of the rolling contact simulation.

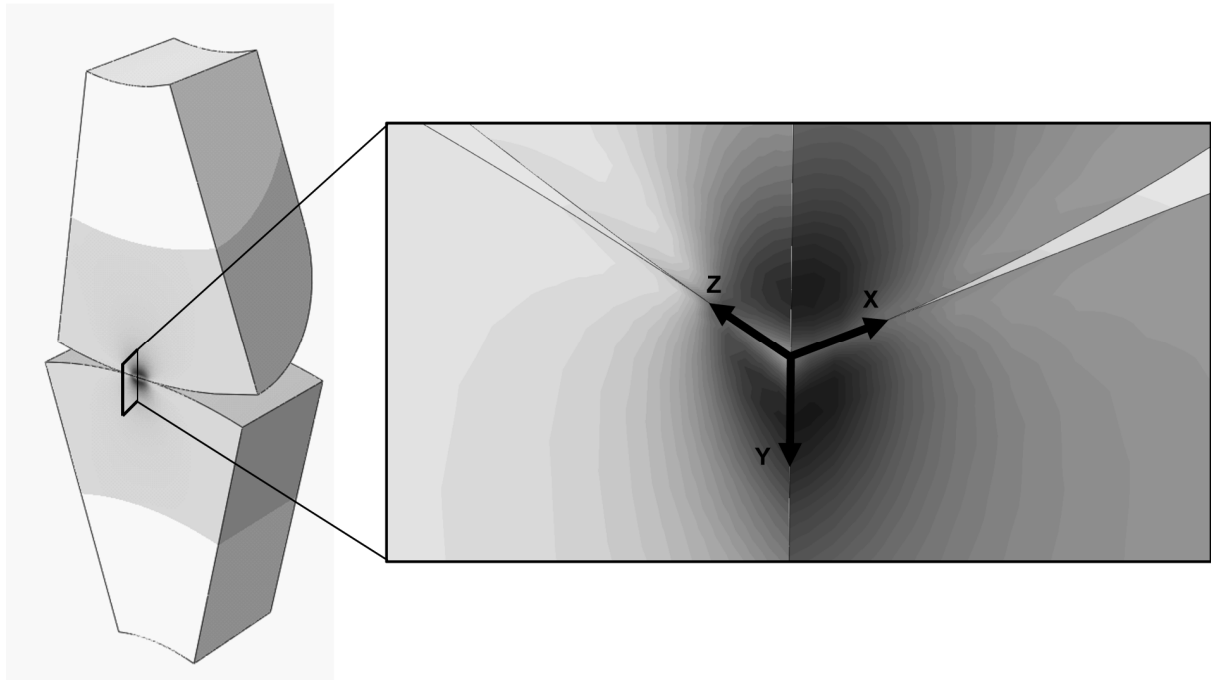|	20°C	100°C
Elastic modulus (GPa)	212	207
Specific heat capacity (J/kg.K)	461	479
Thermal conductivity (W/m.K)	39.6	41.6
Thermal expansion coefficient (K^{-1})	-	12.1×10^{-6}

Figure 2 – Stress nodal data acquired from the X-Y plane parallel to the cutting surface.

2.2 Hydrogen diffusion and trapping model

Detailed descriptions of the finite element formulation of H diffusion and trapping are given elsewhere [7,8,9,10,11]. Here only a brief overview will be given in order to outline the key differences between the past and present routines.

2.2.1 Hydrogen diffusion

The simplest formulation of H diffusion in a stressed lattice in the presence of traps is derived by assuming local equilibrium between H in trap sites and in the surrounding lattice. This assumption enables the H concentration of traps, C_T, to be written as a function of the local lattice concentration,

C_L. Thus, in order to describe the macroscopic redistribution of H in the entire system we need only describe the rate of change of C_L. Assuming isothermal conditions, this is given by [17,18,19]:

$$\frac{dC_L}{dt} = D_{eff}\left(\nabla^2 C_L - \nabla C_L \nabla^2 \sigma_{kk} \frac{V_H}{3kT}\right)$$

Equation 1

where σ_{kk} is the hydrostatic component of the stress, V_H is the partial molar volume of H in solid solution with the bulk lattice and D_{eff} is an effective diffusion coefficient, which is given by:

$$D_{eff} = D_L \frac{C_L}{C_L + C_T(1 - \theta_T)}$$

Equation 2

where D_L is the diffusivity of H in the trap-free lattice and θ_T is the ratio of trapped H atoms to trap sites (i.e. C_T/N_T), which is in turn given by:

$$\theta_T = \frac{1}{\left(1 + \frac{1}{K_T \theta_L}\right)}$$

Equation 3

In which θ_L is the occupancy of lattice sites by H (i.e. C_L/N_L) and K_T is the so-called equilibrium constant. K_T may be defined as the ratio of the characteristic frequencies of H atoms jumping from traps to lattice sites, λ, and from lattice to trap sites, κ, and is given by the Arrhenius expression:

$$K_T = \frac{\kappa}{\lambda} = e^{-\Delta E_T / RT}$$

Equation 4

where ΔE_T is the trap binding energy, which in this case is furnished by analysis of the plastic zone. As per previous continuum studies of H trapping by dislocations [7,8,9,10], a characteristic binding energy of 60kJ/mol [20] was assumed. In actuality, there exists a range of binding energies, perhaps dominated by the activation energies associated with the binding of H to the dislocation core.

2.2.2 Hydrogen trap distribution

In order to characterise the distribution of H traps in the plastic zone, it was assumed that the N_T is proportional to the dislocation density. This was furnished by a simple isotropic hardening model. According to this model, with each consecutive contact pass there is an incremental increase in the local yield stress, given by:

$$\sigma_Y' = \sigma_Y + A\varepsilon_P^b$$

Equation 5

After a few passes and a steady state should be reached after which no further hardening will occur. In this state, σ_Y' is equivalent to the local von Mises stress, σ_M, and the corresponding plastic strain can be approximated by:

$$\varepsilon_P = \left(\left(\sigma_M - \sigma_Y\right)/A\right)^{1/b} \qquad \text{Equation 6}$$

Using the plastic strain, the change in dislocation density may be approximated by Taylor's formula:

$$\rho' = \rho + C\varepsilon_P{}^d \qquad \text{Equation 7}$$

In the present case, A and b were determined by fitting a power-law to the flow curve for 100Cr6 in Hahn et al. [21] to be 1.3×10^{10} N/m^2 and 0.38 respectively. C and d were taken as 1×10^{14} m^{-2} and 1.1 respectively, in line with the range of values given by Yoshida et al. [22]. Figure 5 shows the resulting dislocation distribution along the Y-axis, i.e. passing through the centre of the contact patch. Given the assumed proportionality between N_T and ρ, it follows that:

$$N_T = \frac{\rho' N_b}{b} \qquad \text{Equation 8}$$

Where N_b is the number of trap sites per Burgers vector, b. Kumnick and Johnson [20] estimated values for N_T of between 8.5×10^{20} m^{-3} for annealed Fe and 1.8×10^{23} m^{-3} in 80% cold-rolled Fe. By fitting a power-law to this data, it can be shown that N_T is related to the plastic strain through:

$$N_T = N_{T0} + 2.23 \times 10^{23} \varepsilon_P{}^{1.06} \qquad \text{Equation 9}$$

The similarity of the exponents in Equations 7 and 9 imply that H trap concentration is indeed proportional to the dislocation density, yet the disparity between the multiplicative factors implies that N_b is ~0.3. This gives a value for N_T corresponding to the peak ρ' in Figure 5 of ~4×10^{20}, i.e. in the lower range of the values given by Kumnick and Johnson; however, it is inconsistent with proposals based on DFT calculations that perfectly-straight screw dislocations contain 3 trapping sites per burgers vector [23,24]. Given this disparity and the arbitrary nature of this evaluation, a range of values for N_b between 10^{-1} and 10^{1} were considered in the present study.

2.2.3   Boundary and initial conditions and mesh considerations

The nodal coordinates for a radial plane of the flat roller and the corresponding hydrostatic and von Mises stresses for a single contact pass were exported from the 3D model into a bespoke FE script

programmed in Python. Since the stresses in the plane were symmetrical, the origin was placed at the

centre of the contact ellipse, as shown in Figure 2. The planar mesh was comprised of 90 linear

bilateral elements, with each element corresponding to one face of the tetragonal elements comprising

the 3D model. A small, uniform initial H concentration, C_0, of 10^{23} atoms/m^3 was applied to the mesh

at the beginning of each simulation and maintained at the bulk surfaces for all time. Due to the

uncertainty regarding the mechanism for H generation and ad/absorption, no information pertaining to

H influx was available. Instead, a range of hypothetical boundary conditions were investigated. In the

initial test case, the concentration at the contact surface and the flux at all surfaces were maintained at

zero. In other cases, a constant H concentration was maintained at the wear surface (a width of ~0.26

mm) for all time, whilst the concentration at the remainder of the contact surface was maintained at

zero. The H distribution was computed for 200 time steps for each rotation. Around half of the time

steps occurred in increments of 5×10^{-5} sec during the loading period.

2.2.4   Formulation of finite element equations

The governing differential equation for H diffusion and trapping is derived by applying Green's

theorem to the integral of the weighted residual statement of Equation 1. In matrix form this is given

by [7,8,9,10,11]:

$$\{F\} = [M]\{\dot{C}\} + [K][D_{eff}]\{C\} \qquad\qquad \text{Equation 10a}$$

Where $\{F\}$ is a vector containing the boundary flux, $[D_{eff}]$ is a diagonal matrix containing the nodal

values for D_{eff} and $[K]$ and $[M]$ are the so-called diffusivity and concentration matrices respectively.

$\{F\}$, $[K]$ and $[M]$ are given by:

$$[M] = \int_V [A]^T [A] dV \qquad\qquad \text{Equation 10b}$$

$$[K] = [K_1] + [K_2] + [K_3] \qquad\qquad \text{Equation 10c}$$

$$[K_1] = \int_V [B]^T [B] dV \qquad\qquad \text{Equation 10d}$$

$$[K_2] = \frac{V_H}{3kT} \int_V [B]^T [B]\{\sigma_{kk}\}[A] dV \qquad\qquad \text{Equation 10e}$$

$$[K_3] = \frac{Q_H}{k} \int_V [B]^T [B][T][A]dV \qquad\qquad \text{Equation 10f}$$

$$\{F\} = -\int_S [A]^T \overline{J}dS \qquad\qquad \text{Equation 10g}$$

Where $\{C\}$ and $\{\sigma_{kk}\}$ are the nodal concentration and hydrostatic stress vectors, respectively, $[A]$ and $[B]$ are the standard time-independent interpolation matrices for transient diffusion problems and $\overline{J}$ is the component of the flux normal to the bounding surface S.

Equation 10 was solved using the modified reverse difference method proposed by Sofronis et al. [7]:

$$\left[\frac{1}{\Delta t}[M] + [D_{eff}][K_1]\right]\{C\}_{t+\Delta t} = \frac{1}{\Delta t}[M]\{C\}_t + \{F\}_t - [K_2][D_{eff}/T]\{C\}_t \qquad \text{Equation 11}$$

In order to expedite the routine, $[K_2]$ was pre-computed for each time increment for which external stresses were applied to the plane-of-interest and stored in the computer's working memory.

2.2.5   *Material parameters*

A summary of other material parameters used in the H diffusion and trapping calculations is given in Table 2.

3   Results

Figure 3 shows the maximum hydrostatic stress within the contact patch for a single contact pass (the complete period of rotation is ~0.2 s) calculated using the stress model. In rolling-sliding contact, the hydrostatic and deviatoric components of the contact-induced stresses are separated; the maximum hydrostatic stress occurs at the contact surface in the centre of the contact patch, whereas the maximum von Mises equivalent stress (which includes the deviatoric component) occurs some distance below the surface. Figure 4 shows the distributions of the hydrostatic and von Mises stresses in X-Y plane. In this case the maximum von Mises stress occurs ~160µm below the contact point.

The hydrostatic and von Mises stress field affect the distribution of H in different ways. According to Equation 1, interstitial H diffuses in the direction opposite to the hydrostatic stress gradient, i.e. from the contact surface into the bulk material in an approximately radial direction.

Table 2 – Summary of parameters used in H diffusion and trapping model.

| Parameter		Value	Reference
D_L	Lattice diffusivity	1×10^{-9} m^2/s	
V_H	Partial molar volume of dissolved H	2.3×10^{-6} m^3/mol	25, 30
C_0	Initial H concentration	1×10^{23} atoms/m^3	
Y_0	Initial yield strength	7.45×10^8 N/m^2	21
A	Isotropic hardening coefficient	1.3×10^{10} N/m^2	21
b	Isotropic hardening coefficient	0.38	21
P_0	Initial dislocation density	1×10^{10} m^{-2}	
C	Coefficient for determining P	1×10^{14} m^{-2}	22
d	Exponent for determining P	1.1	22
K_T	Equilibrium trap constant	2.013×10^{-11}	20
N_L	Number of lattice sites	5.1×10^{29} m^{-3}	
b	Burgers vector	0.146×10^{-9} m	
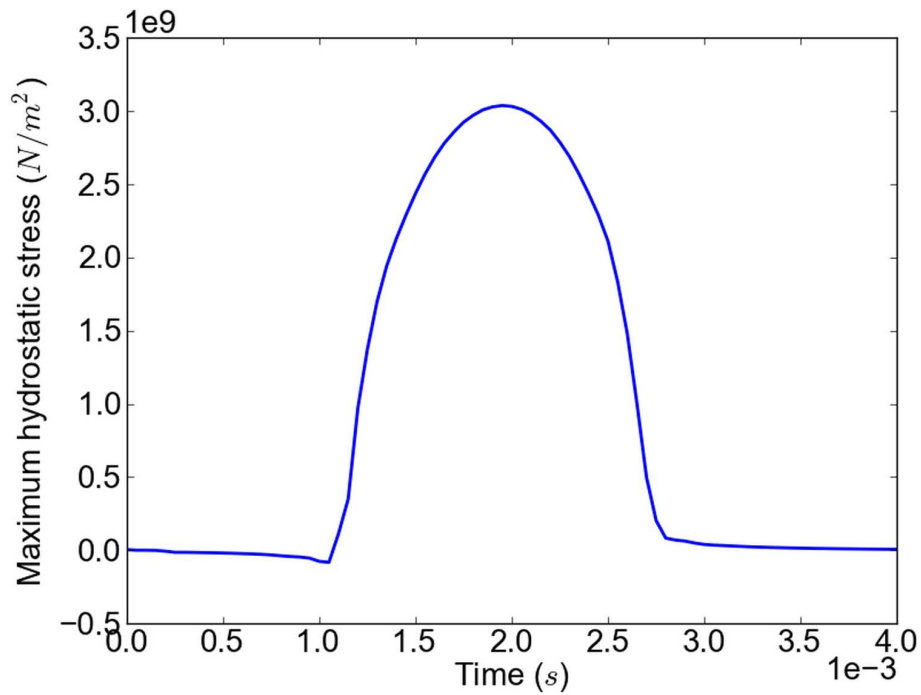
Figure 3 – Maximum hydrostatic stress within the contact patch during one contact pass (complete period of
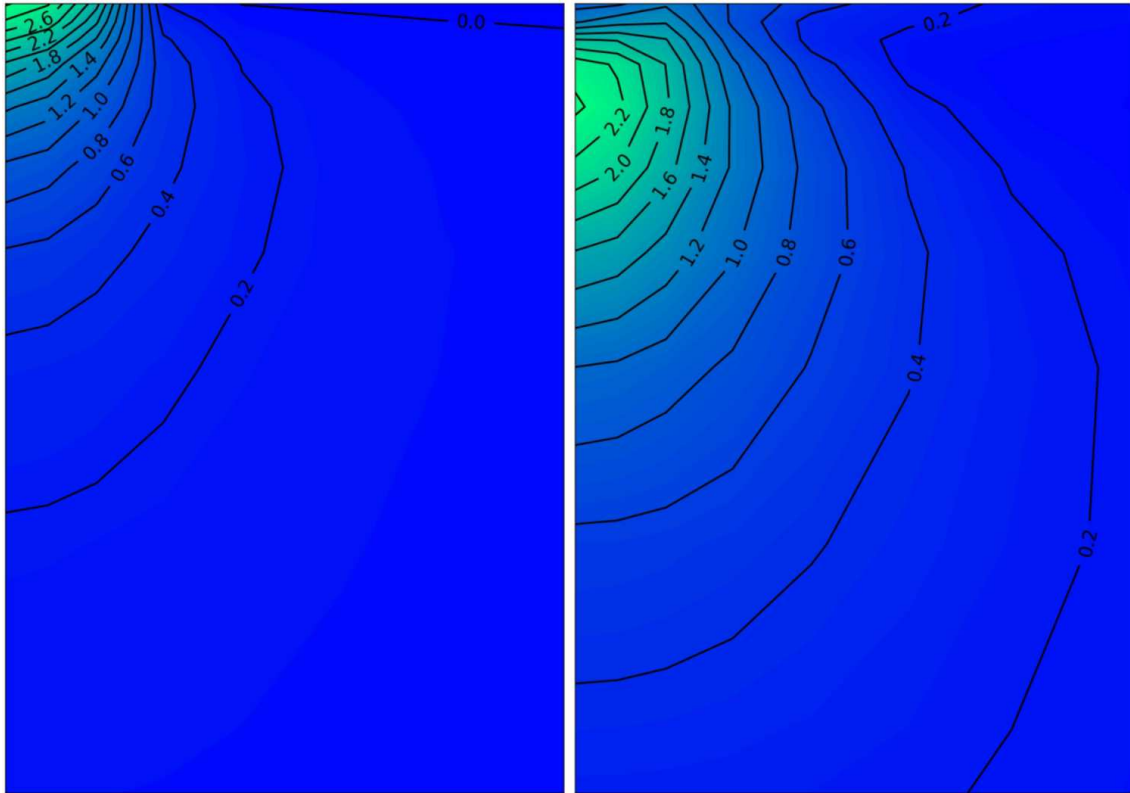
rotation = 0.2 s).

Figure 4 - Hydrostatic (left) and von Mises (right) stresses in a 1.1×1.3 mm region of the X-Y plane with the contact point at the top-left corner (values shown are in ×10^9 N/m2).

According to the hardening model described in Section 2.2.2, the density of dislocations due to plastic deformation, which may behave as H trapping sites, is related to the von Mises stress, such that the maximum dislocation density and the maximum von Mises stress coincide. The approximate increase in dislocation density along the Y-axis due to plastic deformation calculated using the approach is shown in Figure 5.

Figure 6 shows the transient surface temperature along the circumference of the flat roller, assuming an initial temperature of 20°C. For reference purposes, the contact pressure is also shown. There is an increase in the surface temperature of ~22°C due to frictional heating, with the maximum temperature lagging behind the maximum pressure by a distance of ~0.2mm.

Figure 7 shows the total H distribution (i.e. $C_T + C_L$) after 10^4 complete rotations in a 1.1×2mm region of the X-Y plane with the contact point at the top-left corner (assuming N_b=10). The total H concentration is slightly elevated relative to the initial concentration at the point corresponding to the increased dislocation density. The point of maximum H concentration and the contours of the H concentration field correspond with the point of maximum von Mises stress and the size of the plastic

zone (see Figures 4-5) respectively. The change in total H concentration in the plastic zone was also evaluated over various numbers of cycles. Figure 8 shows the H concentration along the Y-axis after $10^0 - 10^4$ complete rotations. It is apparent from Figure 8 that the H concentration in the plastic zone is relatively constant throughout this period.
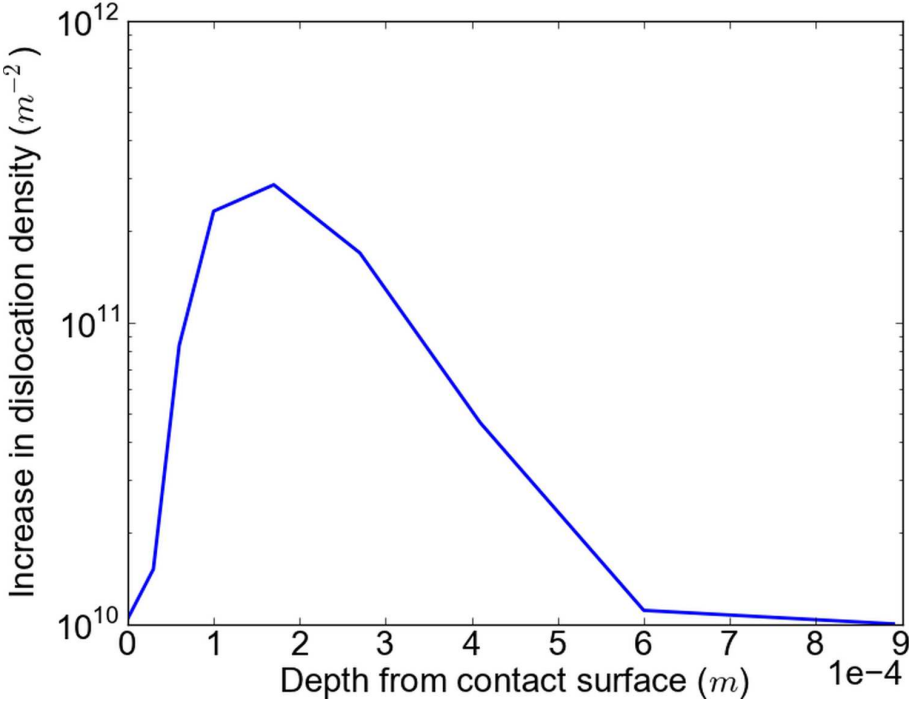

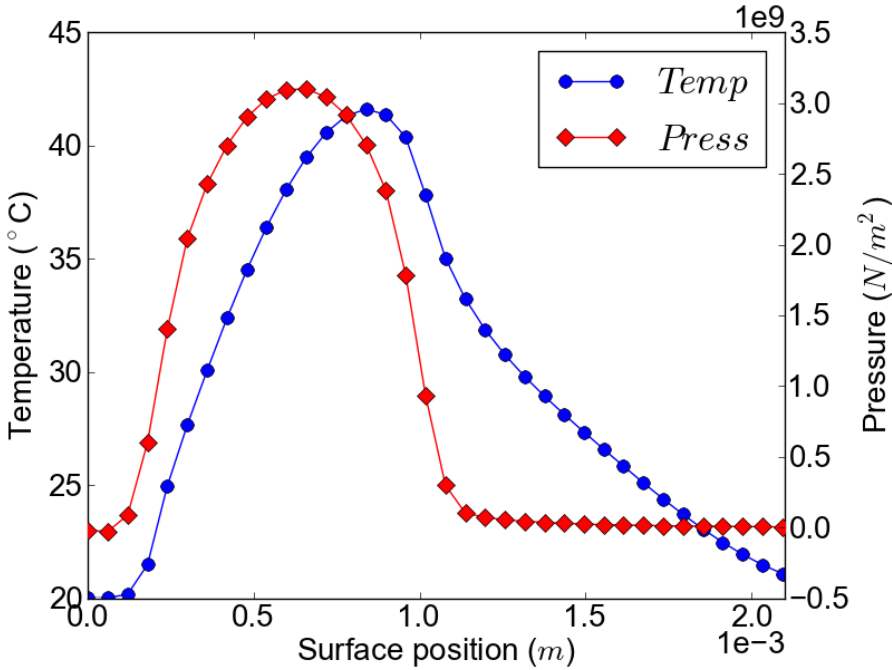*Figure 5 – Increase in dislocation density along the Y-axis as a result of hardening.*

Figure 6 – Transient surface temperature along the circumference of the flat roller. Also shown is the contact pressure, which indicates the instantaneous position of the roller. The rolling direction is from left to right.
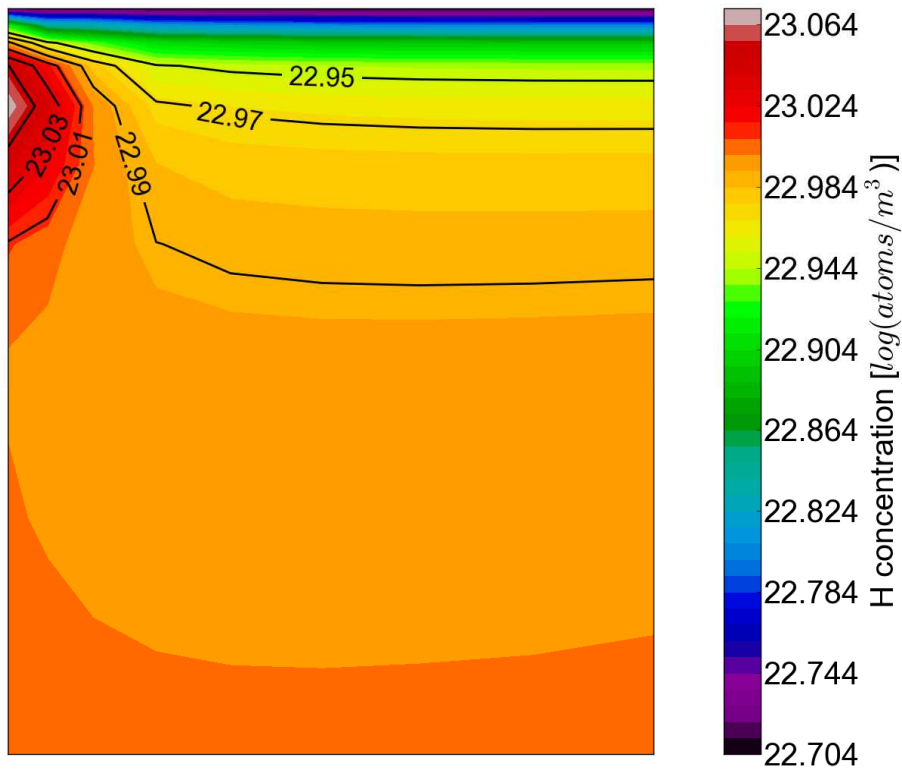
Figure 7 – Total H concentration in a region in a 1.1×1.2 mm region of the plane of interest with the contact point at the top-left corner for Nb=10 after 10^4 complete cycles.
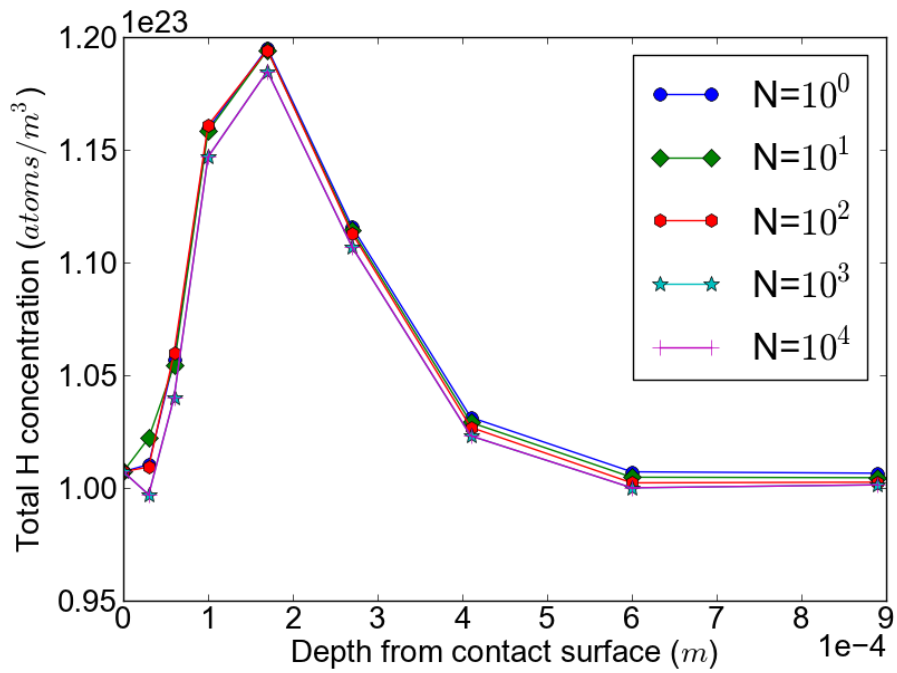

Figure 8 – Total H distribution along the Y-axis after $10^0 – 10^4$ rotations.

Given the uncertainty regarding the trap distribution, a range of values for N_b, the number of traps per Burgers vector of dislocation line, from 0.1 to 10 were evaluated (see Figure 9). In each case, there was an increase in total H concentration relative to the initial concentration, with the H

concentration increasing by ~20% for N_b=10. The point of maximum total H concentration was coincident with the point of maximum von Mises stress (or dislocation density) in all cases.
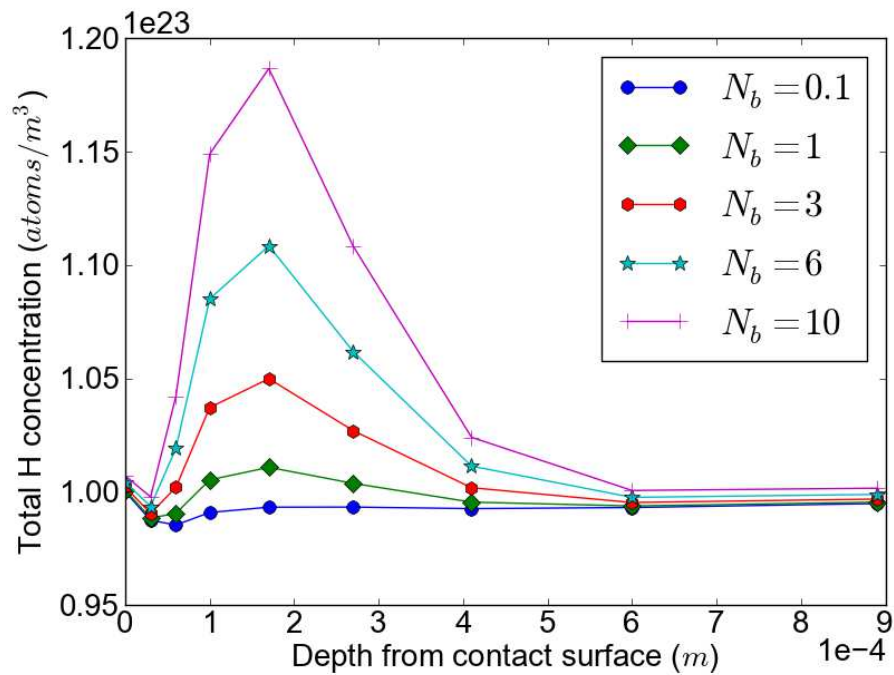

Figure 9 – Total H concentration along Y axis for various values trap densities, characterised by Nb.

The coincidence of the total H concentration with the plastic zone, as well as the independence of the total H concentration from the number of rotations, implies that stress-assisted diffusion of H in normal interstitial lattice sites due to applied contact loads is a relatively small component of the total H flux. Given the shortness of the time-under-load relative to the total period of rotation, it is likely that the H distribution is instead defined by rapid lattice diffusion driven by concentration gradients and H trapping at defects in the plastic zone. In order to test this hypothesis, additional simulations were performed using the same contact stresses but with the period of rotation reduced by a factor of 10. This may occur, for example, in a bearing with multiple rolling elements, albeit with reduced contact stresses. Figure 10 shows that the maximum total H concentration decreases steadily over 10^5 rotations when the period of rotation is reduced; however, the overall reduction in the maximum H concentration in the reduced case is <5%. This is in contrast to the case of a single roller, for which the maximum total H concentration finds a steady-state after 10^3 rotations.
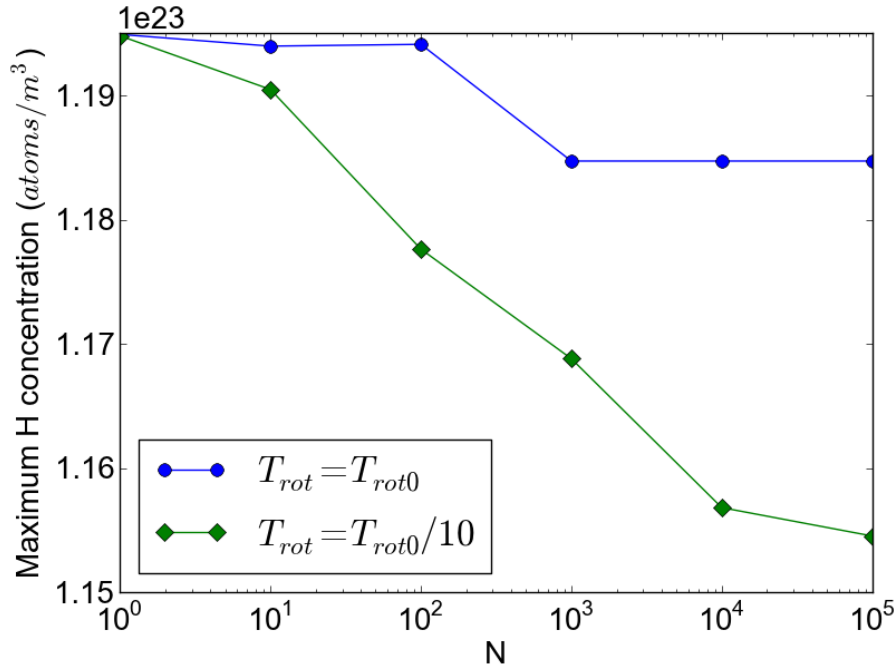
Figure 10 – Maximum total H concentration as a function of the number of cycles for the normal period of rotation and the period of rotation reduced by a factor of 10.

In lieu of any information pertaining to H ingress, various combinations of boundary conditions were evaluated (see Figure 11). In some cases, a constant H concentration of 10^{23} atoms/m^3 or 2×10^{23} atoms/m^3 was maintained at the wear surface, a distance of ~0.26 mm along the X-axis from the origin (whilst the concentration along the remainder of the X-axis was maintained at zero). Static residual stresses were also superimposed onto the cyclic contact stresses in order to evaluate their influence on the near-surface H diffusion. Dommarco et al. [26] measured compressive residual stresses resulting from machining processes of up to 500MPa within a 100µm thick layer at the surface of bearings using X-ray diffraction. In the present model, these stresses were idealised by an exponential decay function:

$$\sigma_R = 5\times10^8 e^{-2.3\times10^4 y} \qquad\qquad \text{Equation 12}$$

The effects of increased H concentration at the wear surface and residual stresses were apparent only in the near-surface region (i.e. y<100µm); neither had a significant influence on the maximum total H concentration. For these calculations was assumed that N_b=100 in order to exaggerate the increase in total H concentration due to trapping.
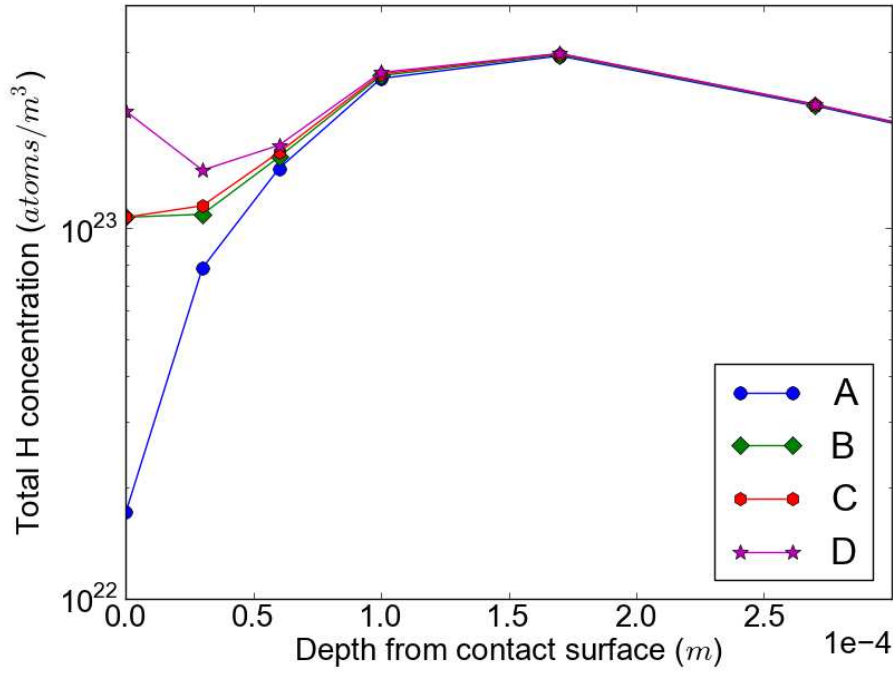
Figure 11 – Total H concentration along the Y-axis for various boundary conditions: (A) without residual stresses or elevated H concentration at wear surface; (B) with constant H concentration (10^{23} atoms/m^3) at wear surface; (C) with residual stresses and constant H concentration (10^{23} atoms/m^3) at wear surface; and (D) with elevated H concentration (2×10^{23} atoms/m^3) at wear surface (Note: N_b=100).

4   Discussion

Notwithstanding the failings of some aspects of this model, in particular the somewhat crude treatment of the hardening behaviour of the material and the arbitrariness of the boundary conditions, it serves to illustrate a key point: that the total H distribution in the bulk material close to the contact zone is relatively unaffected by stress-assisted diffusion under generalised boundary conditions. This is a consequence of: (i) the short period of time a point on the contact surface spends under load relative to the period of rotation; and (ii) the spatial separation of the hydrostatic and von Mises components of the contact stresses. A slight increase in the total H concentration may occur in the plastic zone due to H trapping by deformation-induced defects. Figure 12 shows the components of the steady-state (i.e. after $N=10^4$ cycles) H concentration along the Y-axis corresponding to lattice and trap sites. Also shown for instructive purposes are the hydrostatic, σ_{kk}, and von Mises, σ_v, stresses. A sharp increase in C_T coinciding with the plastic zone, i.e. where $\sigma_v > \sigma_Y$, is apparent, with C_T increasing with σ_v (or trap density – see Figure 5). In contrast, C_L is relatively uniform.
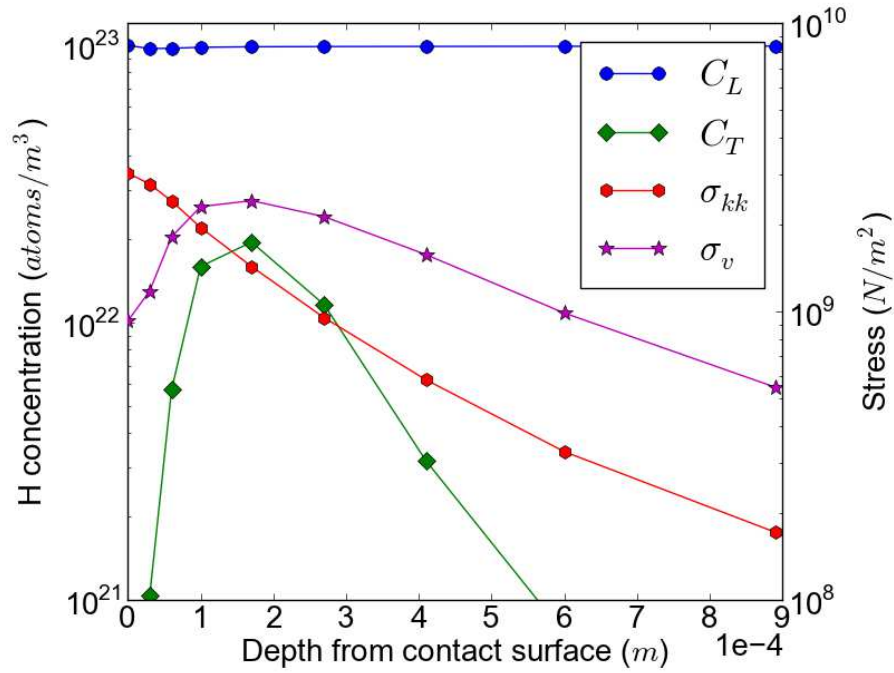
Figure 12 – Steady-state H concentration (i.e. after 10^4 rotations) in lattice, C_L, and trap, C_T, sites with hydrostatic, σ_{kk}, and von Mises, σ_v, stresses.

It is conceivable that the combination of defects (i.e. dislocations and vacancies) and trapped H in the plastic zone would contribute to the acceleration of fatigue processes, i.e. by lowering the activation energy required for localised slip, deformation twinning or even vacancy creep processes [27,28,29]. Very high trap occupancies are possible even when the total increase in H concentration is low: the results shown in Figure 12 indicate that $\theta_T=1$ at the point of maximum von Mises stress. Thus, the results are not inconsistent with an acceleration of fatigue damage processes by absorbed H.

The applicability of the model to lifetime assessment for real bearings would be greatly enhanced by a more rigorous treatment of the hardening behaviour of the material. Detailed hardening models for bearing steels exist in the literature [21], but have been neglected in the present case for the sake of simplicity and computational expediency. Ideally, such models should be incorporated into the specimen-level stress-strain model, although depicting the hardening over multiple cycles may require sacrificing the resolution of the mesh. The applicability of the model to real systems would be greatly improved by the implementation of more realistic boundary conditions. Realistic descriptions of H ingress at the wear surface or residual stresses are highly impracticable; however, a FE model for H diffusion through the remainder of the sample would be relatively straightforward and could be beneficial, depending on the system.

In light of the isotropic hardening model, the assumption that the trap density remains constant for all time seems reasonable. In actuality, it is likely that the so-called "shake down" phase lasts as long as the period for which H is simulated, and that further changes in microstructure and defect distribution occur over even greater numbers of cycles. Thus, a more thorough evaluation of the H distribution over time would take into account changes in the trap density over a larger number of cycles. This would include the decomposition of austenite, which may have a strong influence on the residual stress development [26,30] and damage morphology [27]. The influence of H on the development of the deformation-induced defects cannot be reflected in any model.

The applicability of the model is further limited by the lack of credible experimental data, in particular D_{eff}, the dependence of trap density on plastic strain. The data by Kumnick and Johnson [20], though widely used, may be unsuitable for such materials or indeed for any material under rolling contact conditions. New atomistic methods of evaluating H trapping at defects could also provide insight into the H trapping at deformation-induced defects.

In light of the very low increase in surface temperature due to frictional heating, the description of H diffusion under isothermal conditions would appear to be valid. In any case, this is unlikely to influence the outcome that H distribution is not driven by stress gradients. Temperatures gradients may have a greater influence the absorption, diffusion and trapping of H in systems where more frictional heating occurs.

5   Conclusions

- A preliminary evaluation of H diffusion and trapping in bodies undergoing rolling contact showed only slightly elevated H concentrations may occur in the fatigue process zone. This results is difficult to rationalise with the purported acceleration of fatigue damage processes by absorbed H.

- The accumulation of H is largely defined by the equilibrium concentration of H trapped at deformation-induced defects, rather than by diffusion driven by stress and/or concentration gradients. This is due to: (i) the short period of time a point on the contact surface spends under load relative to the period of rotation; and (ii) the spatial separation of the hydrostatic and von Mises components of the contact stresses.

- Based on these results, it seems reasonable to describe the distribution of H in the near-contact region in terms of the distribution and trapping characteristics of deformation-induced defects. This demands far more rigorous treatment of the hardening behaviour of the material including any microstructural changes that may occur over very large numbers of cycles.

- The applicability of the model to fatigue lifetime evaluation is limited by the unavailability of data pertaining to the trap characteristics of defects occurring under such conditions and the inability to describe the initial and boundary conditions, in particular residual stresses and the mechanism for H generation and absorption.

References

[1]   S. Fujita, S. Matsuoka, Y. Murakami, G. Marquis, Effect of hydrogen on Mode II fatigue crack behavior of tempered bearing steel and microstructural changes, Int. J. Fatigue 32 (2010) 943-951.

[2]   M. Kohara, T. Kawamura, M. Egami, Study on mechanism of hydrogen generation from lubricants, Tribol. T. 49 (2006) 53-60.

[3]   N. Kino, K. Otani, The influence of hydrogen on rolling contact fatigue life and its improvement, JSAE Rev. 24 (2003) 289-294.

[4]   K. Tamada, H. Tanaka, Occurrence of brittle flaking on bearings used for automotive electrical instruments and auxiliary devices, Wear 199 (1996) 245-252.

[5]   H. Hamada, Y. Matsubara, The influence of hydrogen on tension-compression and rolling contact fatigue properties of bearing steel, NTN Technical Review 74 (2006) 54-61.

[6]   J. Gegner, W. Nierlich, Hydrogen accelerated classical rolling contact fatigue and evaluation of the residual stress response, Mater. Sci. Forum 681 (2011) 249-254.

[7] P. Sofronis, R.M. McMeeking, Numerical analysis of hydrogen transport near a blunting crack tip, J. Mech. Phys. Solids 37 (1989) 317–350.

[8] J. Lufrano, P. Sofronis, H.K. Birnbaum, Modelling of hydrogen transport and elastically accommodated hydride formation near a crack tip, J. Mech. Phys. Solids 44 (1996) 179-205.

[9] A.G. Varias, A.R. Massih, Hydride-induced embrittlement and fracture in metals – effect of stress and temperature distribution, J. Mech. Phys. Solids 50 (2002) 1469-1510.

[10] A.H.M. Krom, R.W.J. Koers, A. Bakkar, Hydrogen transport near a blunting crack tip, J. Mech. Phys. Solids 47 (1999) 971-992.

[11] N. Winzer, A. Atrens, D. Dietzel, G. Song, K.U. Kainer, Evaluation of the delayed hydride cracking mechanism for transgranular stress corrosion cracking of magnesium alloys, Mat. Sci. Eng. 466A (2007) 18-31.

[12] G.M. Hamilton, L.E. Goodman, The stress field created by a circular sliding contact, ASME J. Appl. Mech. 33 (1966) 371-376.

[13] G.M. Hamilton, Explicit equations for the stresses beneath a sliding spherical contact, Proc. Instn. Mech. Engrs. 197C (1983) 53-61.

[14] A. Sackfield, D.A. Hills, Some useful results in the classical Hertz contact problem, J. Strain Anal. 18 (1983) 101-108.

[15] A. Sackfield, D.A. Hills, A note on the Hertz contact problem: correlation of standard formulae, J. Strain Anal. 18 (1983) 195-201.

[16] K.L. Johnson, Contact Mechanics, ninth ed. Cambridge University Press, 2003.

[17] A. McNabb, P.K. Foster, A new analysis of the diffusion of hydrogen in iron and ferritic steels, Trans. Met. Soc. AIME. 227 (1963) 618-627.

[18] R.A. Oriani, The diffusion and trapping of hydrogen in steel, Acta Metall. 18 (1970) 147-157.

[19] J.B. LeBlond, D. Dubois, A general mathematical description of hydrogen diffusion in steels – I. Derivation of diffusion equations from Boltzmann type transport equations, Acta Metall. 31 (1983) 1459-1469.

[20] A.J. Kumnick, H.H. Johnson, Deep trapping states for hydrogen in deformed iron, Acta Metall. 28 (1980) 33-39.

[21] G.T. Hahn, V. Bhargava, Q. Chen, The cyclic stress-strain properties, hysteresis loop shape, and kinematic hardening of two high-strength bearing steels, Metall. Trans. 21A (1990) 653-665.

[22] F. Yoshida, A constitutive model of cyclic plasticity, Int. J. Plasticity 16 (2000) 359-380.

[23] M. Wen, S. Fukuyama, K. Yokogawa, Atomistic simulations of effect of hydrogen on kink-pair energetics of screw dislocations in bcc iron, Acta Mater. 51 (2003) 1767-1773.

[24] A. Ramasubramaniam, M. Itakura, M. Ortiz, E.A. Carter, Effect of atomic scale plasticity on hydrogen diffusion in iron: Quantum mechanically informed and on-the-fly kinetic Monte Carlo simulations, J. Mater. Res. 23 (2008) 2757-2773.

[25] L.-C. Hwang, T.-P. Perng, Hydrogen transport in ferritic stainless steel under elastic stress, Mater. Chem. Phys. 36 (1994) 231-235.

[26] R.C. Dommarco, K.J. Kozaczek, P.C. Bastias, G.T. Hahn, C.A. Rubin, Residual stresses and retained austenite evolution in SAE 52100 steel under non-ideal rolling contact loading, Wear. 257 (2004) 1081-1088.

[27] T. Matsumoto, S. Fujita, S. Matsuoka, Y. Murakami, Fatigue crack growth behaviour of a 1900-MPa-class high-strength steel pre-charged with high-pressure hydrogen gas, in: D. Klingbeil, M. Vormwald, K.-G. Eulitz (Eds.), Proc. 18th European Conference on Fracture, DVM, Berlin, 2010, Article No. 637.

[28] R.H. Vegter, J.T. Slycke, The role of hydrogen on rolling contact fatigue response of rolling element bearings, J. ASTM Int. 7 (2009) 1-12.

[29] R. Kirchheim, Reducing grain boundary, dislocation line and vacancy formation energies by solute segregation II. Experimental evidence and consequences, Acta Mater. 55 (2007) 5139–5148.

[30] A.P. Voskamp, Microstructural changes during rolling contact fatigue, PhD Thesis, 1997